Transition metal compounds with S/N-functionalized NHC ligands: structures, redox properties and electrocatalytic activity

Luo, S.; Luo S.

CHAPTER 2

Dinuclear Nickel Complexes of Thiolate-Functionalized Carbene Ligands and their Electrochemical Properties

*Four dimeric nickel(II) complexes $[Ni_2Cl_2(BnC_2S)_2]$ [**1**], $[Ni_2Cl_2(BnC_3S)_2]$ [**2**], $[Ni_2(PyC_2S)_2]Br_2$ [**3**]Br_2 and $[Ni_2(PyC_3S)_2]Br_2$ [**4**]Br_2 of four different thiolate-functionalized N-heterocyclic carbene (NHC) ligands were synthesized and their structures have been determined by single crystal X-ray crystallography. The four ligands differ by the alkyl chain length of the thiolate group (two – C_2 − or three – C_3 − carbon atoms) and the second functionality at the NHC being a benzyl (Bn) or a pyridylmethyl (Py) group. The nickel(II) ions are coordinated to the NHC carbon atom and bridged by the pendant thiolate groups. Additionally, in compounds [**1**] and [**2**] the fourth coordination position of the square-planar Ni(II) centers is occupied by the halide ions, whereas in [**3**]$^{2+}$ and [**4**]$^{2+}$ the additional pendant pyridylmethyl groups complete the coordination spheres of the nickel ions. The electrochemical properties of the four complexes were studied using CV (cyclic voltammetry) and CPC (controlled-potential coulometry) methods. Unfortunately, the thiolate-functionalized carbene complexes [**1**] and [**2**] appear to be poor electrocatalysts for the hydrogen evolution reaction (HER); the complexes [**3**]Br_2 and [**4**]Br_2, bearing an extra pyridylmethyl group, show higher catalytic activity in proton reduction, indicating the pyridine group to play an important role in the catalytic cycle.*

This chapter will be published. S. Luo, M.A. Siegler, and E. Bouwman, submitted

2.1 Introduction

Dihydrogen is a promising fuel which can be used to meet the rapidly increasing global energy demands. It has emerged as a sustainable alternative for fossil fuel resources as upon combustion only water is generated.[1] In general platinum-based electrodes are efficient catalysts for the hydrogen evolution reaction (HER).[2] However, the reserves and price of this noble metal might restrict its application in the future. Hydrogenases are enzymes that efficiently catalyze the transformation between protons and dihydrogen.[3] The abundantly available, non-expensive first row transition metals nickel and iron are present in the catalytic center of these hydrogenases. The coordination of a thiolate sulfur of cysteine to the metal ions in the active site of hydrogenases is likely to play an important role in the activity of the enzyme. Based on this knowledge, chemists worldwide focus their research efforts on mimicking the structure of the active site of hydrogenases. Either two thiolate bridges,[4-8] or a single thiolate bridge[9] are often incorporated in the biomimetic systems. In the search for efficient electrocatalysts for the proton reduction reaction researchers do not limit their investigations to iron and nickel compounds, but also have turned their attention to cobalt,[4] ruthenium,[5] and manganese.[10] Although these systems, such as nickel-bis(diphosphane) catalysts[11-15] and cobaloxime-based catalysts,[16-19] do not mimic the hydrogenase active site, generally these functional models show better electrocatalytic activity than the traditional structural models.[20]

Recently transition metal complexes bearing pyridine-functionalized carbene ligands have been reported as catalysts for HER.[21-23] However, only a few electrochemical studies are related to sulfur-functionalized metal-carbene complexes.[24] In this chapter, we report the synthesis of the dinuclear complexes $[Ni_2Cl_2(BnC_2S)_2]$ [**1**], $[Ni_2Cl_2(BnC_3S)_2]$ [**2**], $[Ni_2(PyC_2S)_2]Br_2$ [**3**]Br_2 and $[Ni_2(PyC_3S)_2]Br_2$ [**4**]Br_2 bearing four different thiolate-functionalized N-heterocyclic carbene (NHC) ligands (Figure 2.1). The thiolate group functions as a bridge between two nickel ions to form dinuclear compounds. The redox properties and electrocatalytic activity in HER of these four compounds are reported.

2.2 Results and Discussion

2.2.1 Synthesis of ligands and complexes

The benzimidazolium precursor salts $[HBnC_2Br]Br$ (**A**) and $[HBnC_3Br]Br$ (**B**),[25] $[HBnC_2SAc]Br$ (**C**) and $[HBnC_3SAc]Br$ (**D**),[26] $[HPyC_2Br]Br$ (**E**) and $[HPyC_3Br]Br$ (**F**)[27] were synthesized following literature methods. The benzimidazolium salts $[HPyC_2SAc]Br$ (**G**) and $[HPyC_3SAc]Br$ (**H**) were synthesized based on literature methods with small modifications (see experimental section).[25, 26] The dimeric nickel compounds $[Ni_2Cl_2(BnC_2S)_2]$ [**1**], $[Ni_2Cl_2(BnC_3S)_2]$ [**2**], $[Ni_2(PyC2S)_2]Br_2$ [**3**]Br_2 and $[Ni_2(PyC_3S)_2]Br_2$ [**4**]Br_2 were obtained from a melt of nickel acetate with the respective acyl-protected ligand precursor (**C**, **D**, **G** and **H**) in tetrabutylammonium bromide under vacuum at 120 °C (see Figure 2.1). The chloride ions in compounds [**1**] and [**2**] are derived from the solvent dichloromethane during the recrystallization process.

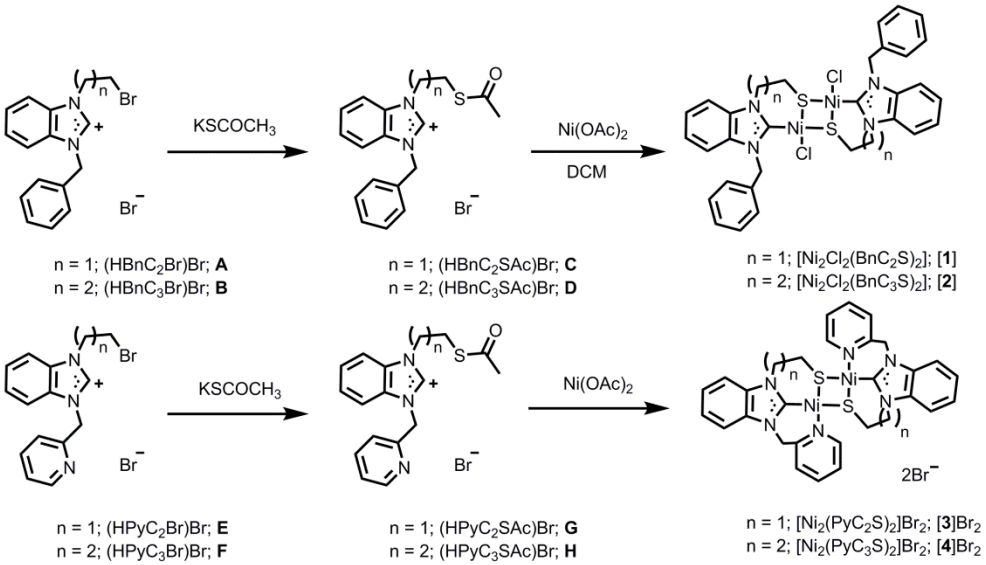

Figure 2.1. Synthesis route of the nickel compounds described in this Chapter.

Deprotonation of the benzimidazolium salt and in situ hydrolysis of the thioester group occurs during the reaction with the nickel salt and the resulting thiolate group bridges between two nickel ions to form the dinuclear Ni-NHC complexes. The four complexes were obtained as red powders. The absence of a ^{1}H NMR signal for the acidic NCHN proton (at ~ 10 ppm) confirmed formation of the desired Ni-carbene bond. The low-spin state of the Ni^{II} ions in compounds [**1**], [**2**] and [**4**]Br_2 is evidenced by their diamagnetic ^{1}H NMR spectra. In contrast, the ^{1}H NMR spectrum of compound [**3**]Br_2 in DMSO-d_6 shows rather broad signals (Figure AII.1). Low temperature NMR spectra could not be obtained as the solvent DMSO-d_6 is not suitable. ESI-MS analysis of the four compounds shows the presence of dicationic fragment ions $[M-2X]^{2+}$ and $[M-X]^+$. Despite the fact that recrystallized samples of the Ni compounds were dried in vacuo before elemental analysis was performed, the analytical data still show the presence of the solvents that were used in recrystallization.

2.2.2 Structural characterization of the complexes

Single crystals of [**1**] and [**2**] suitable for X-ray structure determination were obtained from slow evaporation of dichloromethane solutions of the compounds. Solutions of the complexes [**3**]Br_2 and [**4**]Br_2 are not stable in air (Figure AII.2); the compounds slowly decompose as apparent by a color change. Single crystals of these two complexes suitable for X-ray structure determination were obtained by slow evaporation of degassed methanol solutions under a flow of argon. The crystallographic data of compounds [**1**], [**2**], [**3**]Br_2 and [**4**]Br_2 are collected in Table AII.1 in Appendix II; selected bonds lengths and angles are given in Table 2.1. Projections of the structures are shown in Figure 2.2.

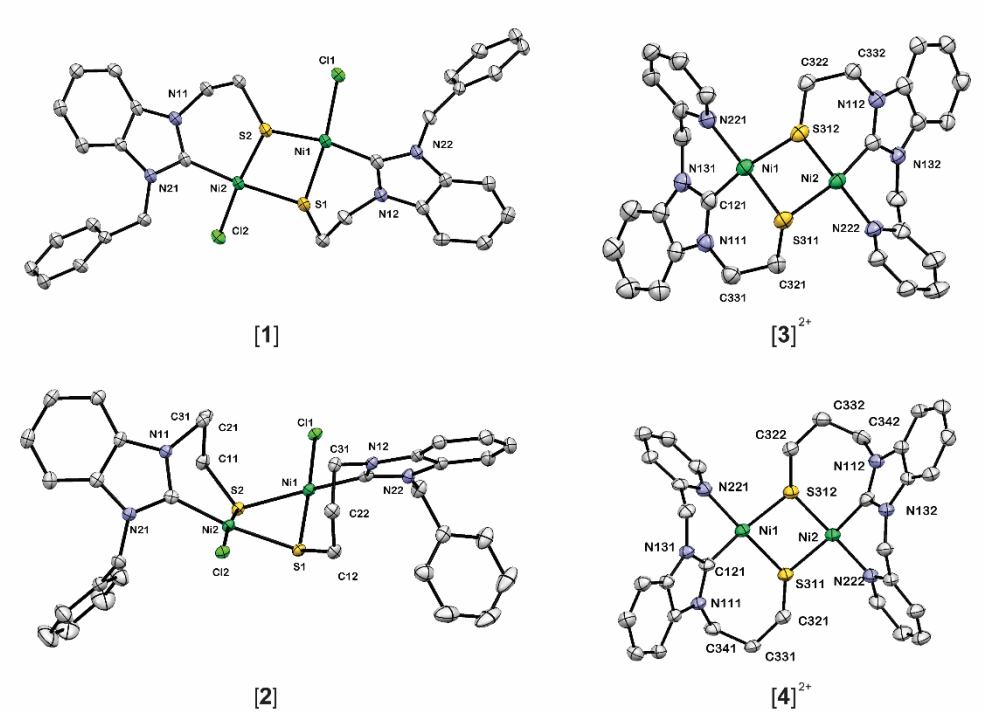

Figure 2.2. Displacement ellipsoid plots of the cationic compounds: [1], [2], $[3]^{2+}$ and $[4]^{2+}$ drawn at 50% probability level with selected atom numbering. Hydrogen atoms, non-coordinated bromide ions and lattice solvent molecules are omitted for clarity.

In the structures of compounds [**1**] and [**2**], each Ni center is coordinated by the bidentate ligand via the NHC carbon atom and the thiolate sulfur of the pendant arm as well as one chloride ion; the coordination sphere of the Ni^{II} ions is completed by a bridging thiolate donor of a second monomeric unit, resulting in the observed dinuclear structure. Thus the coordination geometry of the nickel ions in compounds [**1**] and [**2**] can be described as slightly distorted square planar (τ_4 = ~0.16 for [**1**], τ_4 = ~0.13 for [**2**]; τ_4 = 0 being the theoretical value for an ideal square-planar geometry).[28]

The nickel ions in [**3**]Br_2 and [**4**]Br_2 are coordinated by the tridentate ligand, bound via the pyridyl nitrogen, the NHC carbon and thiolate sulfur atom; the coordination sphere of the nickel centers is completed by a bridging thiolate sulfur atom of a second nickel center, thus forming the dinuclear complexes. The square-planar geometry of the nickel centers in $[\mathbf{3}]^{2+}$ and $[\mathbf{4}]^{2+}$ is even less distorted than those in [**1**] and [**2**] as evidenced by the smaller τ_4 values (τ_4 = ~0.10 for $[\mathbf{3}]^{2+}$, ~0.07 for $[\mathbf{4}]^{2+}$).

The crystal structure of compound [**1**] with two bromide ions instead of chlorides has been reported in the non-centrosymmetric orthorhombic $P2_12_12_1$ space group,[29] while compound [**1**] crystallized in the centrosymmetric triclinic *P-1* space group even though the environments of the nickel centers are highly similar. The bond distances and angles in [**1**]

are comparable with those in the published structure,[29] with the logical exception that the Ni─Cl bond is shorter than the Ni─Br distance. The complexes [**2**], [**3**]Br_2, and [**4**]Br_2 present similar Ni─C and Ni─S bond lengths. The Ni─C bond lengths in the four complexes are all around 1.89 Å and the Ni─S bond lengths within the chelating ligand are around 2.15 ~ 2.18 Å. The Ni─S bond distances to the thiolate sulfur of the other nickel center are slightly longer, namely around 2.19 ~ 2.22 Å. The Ni─N bond lengths in $[\mathbf{3}]^{2+}$ and $[\mathbf{4}]^{2+}$ are 1.929 Å and 1.922 Å, respectively.

*Table 2.1. Selected bond distances (Å) and angles (°) of the compounds [**1**], [**2**], [**3**]Br_2 and [**4**]Br_2.*[a]

	[**1**]	[**2**]	[**3**]Br_2	[**4**]Br_2
Ni1–S	2.1736(9)	2.1743(7)	2.153(3)	2.1829(15)
Ni1–S'	2.2312(9)	2.2227(6)	2.227(4)	2.2084(16)
Ni1–C	1.883(4)	1.887(2)	1.889(9)	1.882(6)
Ni1–Cl1	2.1943(9)	2.2046(6)	/	/
Ni1–N	/	/	1.930(8)	1.922(4)
Ni1…Ni2	3.0847(8)	3.0413(6)	2.960(4)	3.068(1)
S–Ni1–S'	77.77(4)	78.15(2)	79.22(14)	79.92(6)
S–Ni1–C	90.72(11)	94.00(7)	94.8(3)	97.34(16)
S'–Ni1–C	165.60(11)	169.67(7)	165.4(4)	169.03(17)
S–Ni1–Cl	172.34(4)	172.32(3)	/	/
S'–Ni1–Cl	96.03(4)	96.61(2)	/	/
C–Ni1–Cl	96.06(11)	91.84(7)	/	/
S–Ni1–N	/	/	163.5(3)	167.46(15)
S'–Ni1–N	/	/	96.1(3)	95.13(15)
C–Ni1–N	/	/	93.2(4)	89.6(2)
Dihedral angle α	44.5(3)	66.9(2)	10.6(5)	24.9(6)
Hinge angle β	128.24(5)	125.99(4)	119.54(7)	130.44(8)

[a] *S = S1 ([**1**] and [**2**]), S311 ([**3**]Br_2 and [**4**]Br_2); S' = S2 ([**1**] and [**2**]), S312 ([**3**]Br_2 and [**4**]Br_2); C = C91 ([**1**]), C101 ([**2**]), C121 ([**3**]Br_2 and [**4**]Br_2); Cl = Cl1 ([**1**] and [**2**]); N = N221 ([**3**]Br_2 and [**4**]Br_2);.*

In order to compare the surroundings of the four complexes in detail, the dihedral angle α and hinge angle β are defined (Figure 2.3). The dihedral angle α is the torsion angle N–C–Ni–S, describing the angle between the plane of the benzimidazolidene ring and the square plane of the nickel center, indicating the orientation of the carbene ligand with respect to the plane of coordination. The hinge angle β is the torsion angle Ni–S–S'–Ni', describing the dihedral angle between the two adjacent coordination planes of the nickel centers, indicating the bent nature of the dinuclear molecule. Of the four complexes, the complexes [**3**]Br_2 and [**4**]Br_2 show much smaller dihedral angles α than [**1**] and [**2**], indicating that the presence of the third donor atom (the pendant pyridyl group) forces the NHC ring to orient itself in a more co-planar fashion with the plane of coordination. In general, the NHC carbene ligand preferentially is oriented perpendicular to the plane of coordination with dihedral angles α between 40-90°.[28, 30-34] Few exceptions have been reported for complexes bearing certain type of tridentate pincer ligands.[35-37]

Notably, the complex $[Ni_2(PyC2S)_2]Br_2$ [**3**]Br_2 not only displays the smallest torsion angle α (10.6(5)°), but also smallest hinge angle β (119.54(7)°). This means that this molecule is

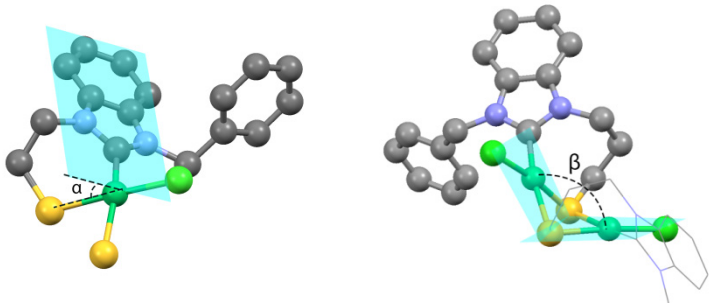

Figure 2.3. Schematic diagrams of the dihedral angle α and hinge angle β.

equipped with two nearly flat "wings", but that the overall structure is significantly bent. The crystal packing of compound [**3**]Br_2 shows an interesting interaction between one of the bromide ions with two dinuclear cations: two bent dinuclear molecules form a Ni_4S_4 "box" encapsulating the bromide ion (see Figure 2.4). This bromide ion is located near the apical position of each square-planar nickel center, with Ni to Br distances ranging between 3.4 to 3.6 Å (Ni1…Br1 = 3.616(3) Å, Ni2…Br1 = 3.668(5) Å, Ni3…Br1 = 3.422(5) Å, Ni4…Br1 = 3.403(6) Å). This interaction between four Ni centers and the bromide ions holds the Br^- ion in the center of a distorted "Ni_4 tetrahedron". If this supramolecular interaction is retained in solution it might be the cause of the broadening observed in the proton NMR spectrum of this compound.

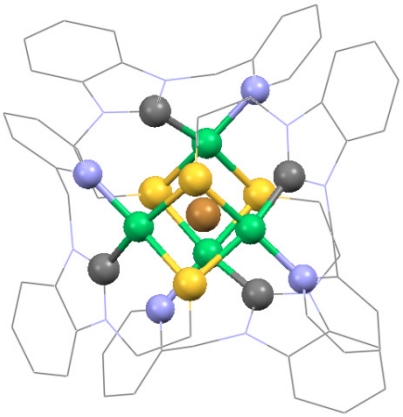

*Figure 2.4. Projection of the interaction between two [**3**]$^{2+}$ cations and one bromide ion in the crystal structure of compound [**3**]Br_2. Different elements are distinguished by color: nickel (green), sulfur (yellow),nitrogen (blue), carbon (grey), and bromide (brown).*

2.2.3 Electrochemical properties of the complexes

The redox properties of the two compounds $[Ni_2Cl_2(BnC_2S)_2]$ [**1**] and $[Ni_2Cl_2(BnC_3S)_2]$ [**2**] were first investigated with cyclic voltammetry in dry DMF solutions containing 0.1 M

tetrabutylammonium hexafluoridophosphate (TBAP) as the supporting electrolyte under a stream of argon. The CV of complex [**1**] shows one large irreversible reductive peak at −1.20 V followed by a more or less reversible couple at $E_{1/2}$ = −1.96 V vs Ag/AgCl. In between these reduction events two smaller reduction peaks are present (Figure 2.5). The CV of complex [**2**] shows a similar irreversible reductive peak at −1.28 V vs Ag/AgCl, at a slightly more negative potential compared to the C_2 analogue.

With the aim to study the electrocatalytic activity of these compounds in HER, subsequently acetic acid was added into the solutions of [**1**] and [**2**]. As a result, an increase in the current with an onset potential around −1.60 V was observed, but in both experiments only weak catalytic currents were observed (Figure 2.6).

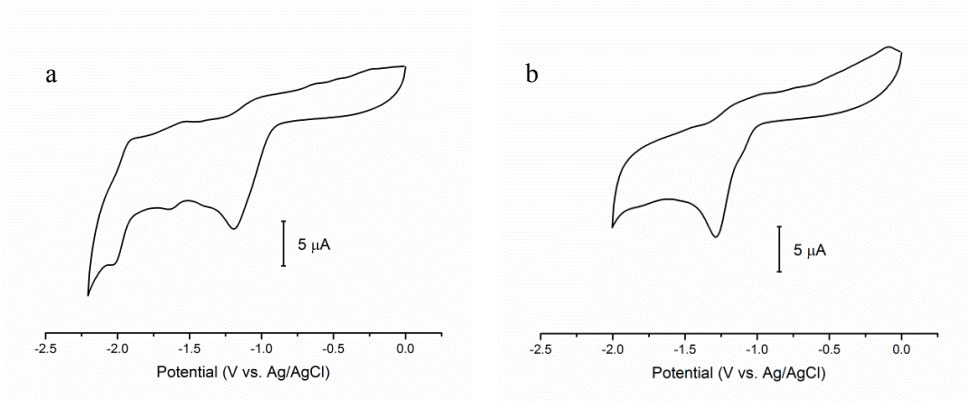

*Figure 2.5. The CVs of complexes [**1**] (a) and [**2**] (b) recorded in DMF containing 0.1 M TBAP as supporting electrolyte at scan rate 0.1 V/s, using glass carbon as working electrode.*

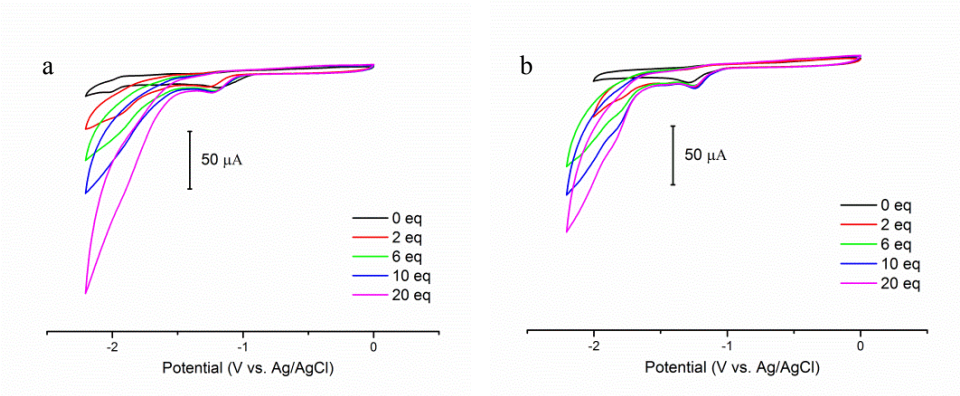

*Figure 2.6. The CVs of complexes [**1**] (a) and [**2**] (b) recorded in presence of various equivalents of acetic acid in DMF containing 0.1 M TBAP as supporting electrolyte at scan rate 0.1 V/s, using a glassy carbon working electrode.*

The redox properties of the pyridyl-containing complexes [**3**]Br_2 and [**4**]Br_2 were also investigated with cyclic voltammetry. In absence of acid, complex [**3**]Br_2 showed a number

of irreversible peaks with similar current intensities located in the range of −0.7 to −1.6 V, followed by a more or less reversible reduction at $E_{1/2}$ = −1.95 V vs. Ag/AgCl (Figure AII.4). The first reductive peak at −0.9 V becomes more reversible upon increasing scan rates (Figure 2.7). The complex [**4**]Br_2 with the longer alkyl chain shows a similar complicated CV (Figure AII.4). Similar to complex [**3**]Br_2, the first reductive peak becomes more reversible at higher scan rates (Figure 2.7). Notably, the first redox event of [**3**]Br_2 ($E_{1/2}$ = −0.88 V) occurs at more positive potential compared to the one of [**4**]Br_2 ($E_{1/2}$ = −0.98 V).

The complicated irreversible CVs of complex [**3**]Br_2 and [**4**]Br_2 might be due to solvation reactions in solution, resulting in an equilibrium of dimeric and monomeric species as shown in Figure 2.8. The dimeric structure might partly break up in solution after which the nickel ion coordinates with a bromide ion or solvent molecule to form a monomeric compound. The dimeric species and the different monomeric species will be reduced at different potentials, resulting in the multiple reductive waves. Alternatively, two Ni(II) ions in the dinuclear structure may successively be reduced to Ni(I) and then to Ni(0) instead of simultaneously.

Upon addition of acetic acid into the DMF solutions containing complex [**3**]Br_2 or [**4**]Br_2, a totally different electrochemical response is obtained compared to the complexes [**1**] and [**2**]. Whereas for complex [**1**] or [**2**] no obvious catalytic current was observed, upon addition of acetic acid into the DMF solution containing complex [**3**]Br_2, the reductive current after the onset potential of −0.91 V gradually increased; a large reductive current peak is observed at around −2 V. The solution of complex [**4**]Br_2 showed a similar result in presence of acetic acid with a onset potential at −1.08 V (Figure 2.9). In both situations, with increasing concentrations of acid the reductive current increased linearly (Figure 2.10). The i_c/i_p ratio is 100 for [**3**]Br_2 and 85 for [**4**]Br_2 in presence of 130 mM acid. Here, i_c is the maximum current of the catalytic peak, and i_p is the plateau current of the non-catalytic reduction wave.

Plots of i_c/i_p versus the square root of acid concentration for complexes [**3**]Br_2 and [**4**]Br_2 show a non-linear relationship (Figure AII.5). Instead, a linear relationship is found between i_c/i_p versus the acid concentration (Figure 2.10); thus the reaction is second order in acid, indicating that two protons are involved in the rate-determining catalytic step. The rate constant k_{obs} of the compounds cannot be calculated using equation (1)[6, 12, 13, 38-40] or the foot-of-the-wave method, as the preceding reduction wave is not reversible.[41-44]

$$\frac{i_c}{i_p} = \frac{n}{0.4463}\sqrt{\frac{RTk_{obs}}{Fv}} \quad (1)$$

By comparison of the i_c/i_p ratio it seems that complex [**3**]Br_2 shows higher catalytic activity in HER. However, complex [**3**]Br_2 also presents a redox process at $E_{1/2}$ = −1.95 V, which significantly overlaps with the catalytic current. Considering this redox event of the complex, the catalytic activity in this case might be lower than expected from the i_c/i_p ratio.

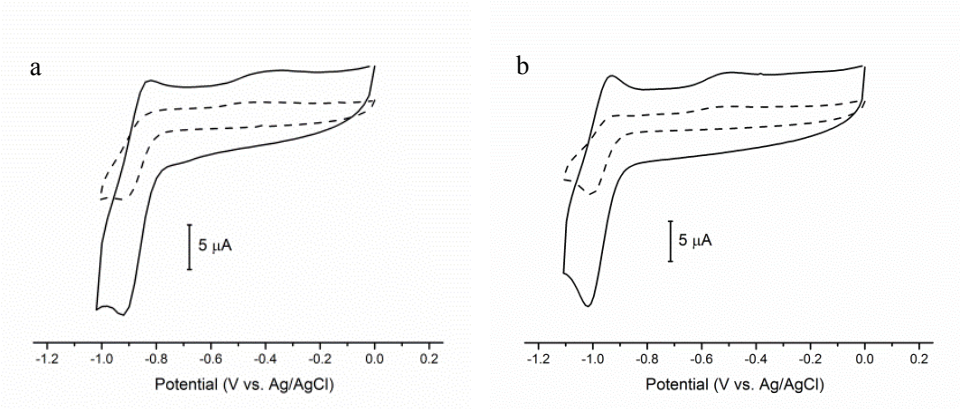

*Figure 2.7. Cyclic voltammograms of 1 mM [**3**]Br_2 (a) and [**4**]Br_2 (b) recorded in DMF containing 0.1 M TBAP as supporting electrolyte at different scan rates (dashed line = 0.1 V/s; solid line = 0.5 V/s), using a glassy carbon working electrode.*

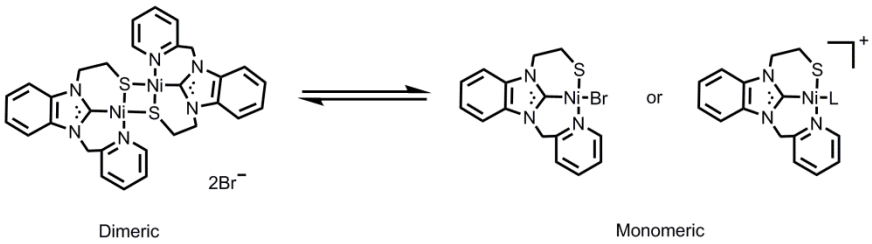

*Figure 2.8. Proposed dimer-monomer equilibrium of [**3**]Br_2 in solution (L = N,N-dimethylformamide).*

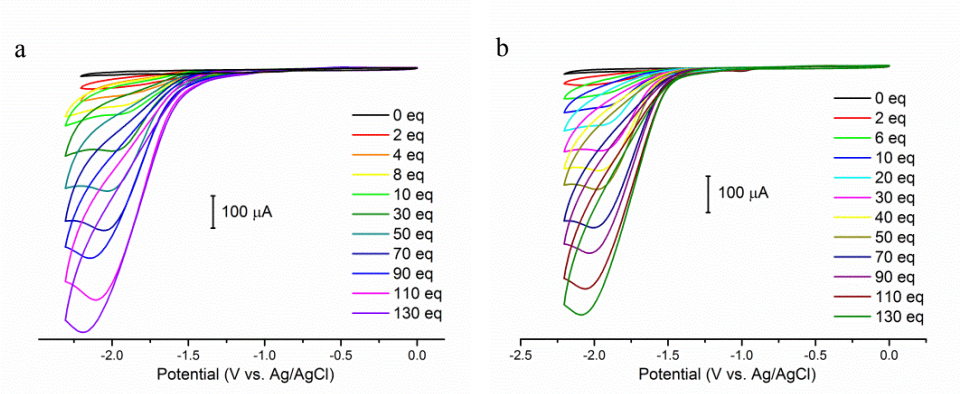

*Figure 2.9. The CVs of complexes [**3**]Br (a) and [**4**]Br (b) recorded in presence of various equivalents of acetic acid in DMF containing 0.1 M TBAP as supporting electrolyte at scan rate 0.1 V/s, using a glassy carbon working electrode.*

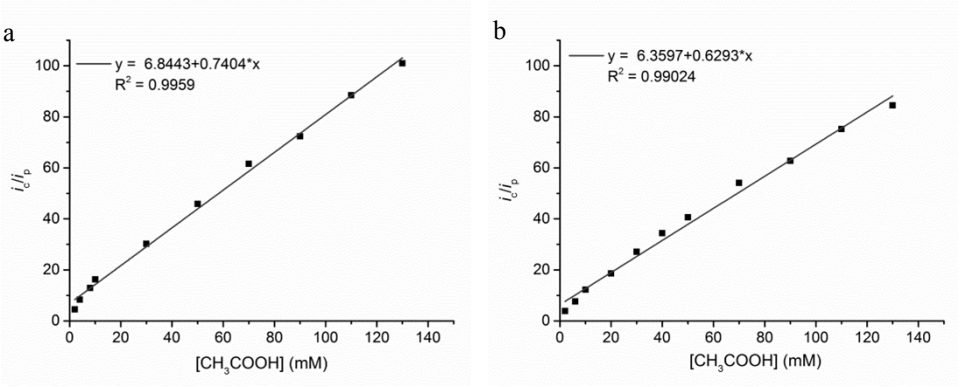

*Figure 2.10. Plot of i_c/i_p vs. [CH_3COOH] (mM) for [**3**]Br_2 (a) and [**4**]Br_2 (b). Conditions:1 mM complex in DMF containing 0.1 M TBAP as supporting electrolyte at 0.1 V/s, using a glassy carbon working electrode.*

With the aim to compare the electrocatalytic activity of the four compounds in a more quantitative way, controlled-potential coulometry experiments (CPC) were carried out. The charge consumptions over time of solutions containing just the pure acid or each of the catalysts were also recorded separately as references. The charge accumulation graphs show that over a period of 10 minutes charge consumption is negligible for the solutions containing only acid or only the nickel compounds (Figure 2.11 and Figure AII.6). In contrast, for solutions containing both acid and one of the nickel catalysts continuous charge consumption was recorded. Although no clear catalytic peaks were observed in the CV experiments for complex [**1**] or [**2**] in the presence of acid (Figure 2.6), relatively high charge consumptions were observed in the CPC experiments (Figure 2.11 and Figure AII.6). As expected, the pyridine-functionalized compounds [**3**]Br_2 and [**4**]Br_2 resulted in higher charge consumptions, indicating higher catalytic activities. The quantity of dihydrogen generated during the CPC experiments can be estimated from the charge consumption of solutions containing both the nickel compound and the acid after subtraction of the charge consumption of the blanks; the results are listed in Table 2.2 (assuming that all electrons are used in proton reduction). Among the four complexes, the compound $[Ni_2(PyC_3S)_2]Br_2$ [**4**]Br_2 shows the highest catalytic activity, which is estimated to produce 5×10^{-4} mmol H_2 gas in 10 min in presence of 6×10^{-3} mmol catalyst at a potential of −1.80 V. These compounds can hardly be considered to be good catalysts for HER; even so, it is apparent that the pyridine-functionalized complexes $[Ni_2(PyC_2S)_2]Br_2$ [**3**]Br_2 and $[Ni_2(PyC_3S)_2]Br_2$ [**4**]Br_2 as catalysts perform better than their benzyl-substituted analogues.

Table 2.2. Estimated amount of dihydrogen generated by the four compounds in 10 minutes ($n_{catalyst}$ = 6×10^{-3} mmol).

Compound	$[Ni_2Cl_2(BnC_2S)_2]$ [**1**]	$[Ni_2Cl_2(BnC_3S)_2]$ [**2**]	$[Ni_2(PyC_2S)_2]Br_2$ [**3**]Br_2	$[Ni_2(PyC_3S)_2]Br_2$ [**4**]Br_2
n (H_2) (mmol)	1.5×10^{-4}	1.5×10^{-4}	4×10^{-4}	5×10^{-4}

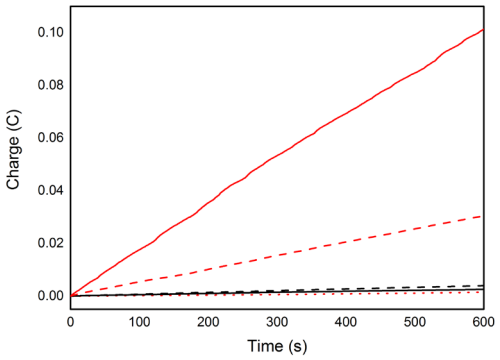

*Figure 2.11. Charge vs. time plot over 600 s during CPC at a potential of −1.8 V. Black line: compounds in absence of acid; Red line: compounds in presence of 50 mM acetic acid (dashed = 1 mM [$Ni_2Cl_2(BnC_3S)_2$] [**2**], solid = 1mM [$Ni_2(PyC_3S)_2$]Br_2 [**4**]Br_2); Dotted red line: 50 mM acetic acid only.*

2.3 Conclusion

In this Chapter, the synthesis and characterization is reported of the compounds [$Ni_2Cl_2(BnC_2S)_2$] [**1**], [$Ni_2Cl_2(BnC_3S)_2$] [**2**], [$Ni_2(PyC_2S)_2$]Br_2 [**3**]Br_2 and [$Ni_2(PyC_3S)_2$]Br_2 [**4**]Br_2, comprising four different thiolate-functionalized N-heterocyclic carbene ligands. CV and CPC experiments were used to investigate the redox properties and electrocatalytic activity of these complexes. In this Chapter, for thiolate-functionalized carbene compounds [**1**] and [**2**], we observed their weak catalytic activity on HER. However, it was found that compounds [**3**]Br_2 and [**4**]Br_2 containing pyridine groups show better catalytic activity in HER than their benzyl-containing analogues. Unfortunately, the limited stability of solutions of the complexes [**3**]Br_2 and [**4**]Br_2 in presence of air and the low electrocatalytic efficiency limit their potential application as proton reduction catalysts. Meanwhile understanding of the role of thiolate and pyridine group in catalytic cycle still requires further related research, which may help the design of efficient biomimic catalysts on HER.

2.4 Experimental

2.4.1 Materials

Commercial chemicals were used without further purification. Acetonitrile and diethyl ether were obtained from a PureSolv MD5 solvent dispenser. Dry dimethylformamide were prepared by adding molecular sieves into commercial anhydrous solvent. The rest commercial solvents were used without further purification. All air-sensitive reactions were performed under argon or dinitrogen gas using standard Schlenk techniques unless mentioned otherwise.

2.4.2 Analytical methods

^{1}H and ^{13}C spectra were recorded on a Bruker 300 DPX spectrometer. Mass spectra were obtained using a Finnigan Aqua Mass Spectrometer (MS) with electro spray ionization (ESI). UV-vis spectra were obtained using a transmission dip probe using an Avantes Avaspec-2048 spectrometer with an Avalight-DH-S-BAL light source. Elemental analyses were performed by the Kolbe Mikroanalytisches Laboratorium, Germany.

Cyclic voltammetry was recorded with an Autolab PGstat10 potentiostat controlled by GPES4 software under argon. A 3 mm diameter glassy carbon electrode was used as working electrode and platinum as the counter electrode. The cyclic voltammetry was performed in dry DMF with 0.1 M tetrabutylammonium hexafluoridophosphate (TBAP) as the supporting electrolyte under a stream of argon at room temperature. The experimental reference was an Ag/AgCl (3 M KCl) electrode in the electrolyte solution (TBAP). Ferrocene was added at the end of each measurement as an internal standard. Under these conditions the Fc/Fc^{+} couple was located at 0.510 V vs Ag/AgCl with a ΔE_p of 95 mV. The surface of the working electrode was polished, sonicated and rinsed before each single CV measurement.

Controlled-potential coulometry (CPC) experiments were carried out with an Autolab PGstat10 potentiostat controlled by GPES4 software under argon. A 3 mm diameter glassy carbon electrode was used as working electrode and platinum as the counter electrode. 0.006mmol complex (1 mM) and 17.5 µL acetic acid (50 mM) were added in 6 mL dry degassed DMF with 0.1 M tetrabutylammonium hexafluoridophosphate (TBAP) as the supporting electrolyte under a stream of argon at room temperature. A CPC experiment was run at −1.8 V for 600 s, while the solution was stirred continuously. The blank and reference CPC experiments (only acid or only catalyst added) were performed using the same conditions.

3.4.3 Single Crystal X-ray Crystallography

All reflection intensities were measured at 110(2) K using a SuperNova diffractometer (equipped with Atlas detector) with Cu *K*α radiation (λ = 1.54178 Å) under the program CrysAlisPro (Versions 1.171.36.32, 1.171.37.31 or 1.171.37.35 Agilent Technologies, 2013-2014). The same program was used to refine the cell dimensions and for data reduction. The structure was solved with the program SHELXS-2013,[45] and was refined on F^2 with SHELXL-2013.[45] Analytical numeric absorption corrections based on a multifaceted crystal model were applied using CrysAlisPro. The temperature of the data collection was controlled using the system Cryojet (manufactured by Oxford Instruments). The H atoms were placed at calculated positions (unless otherwise specified) using the instructions AFIX 23, AFIX 43, AFIX 137 or AFIX 147 with isotropic displacement parameters having values 1.2 or 1.5 *U*eq of the attached C atoms. For [**4**]Br_2, the H atoms attached to O1W were found from difference Fourier maps, and their coordinates were refined freely.

$[Ni_2Cl_2(BnC_2S)_2]$ [**1**]: The structure is disordered. The crystal that was mounted on the diffractometer was non-merohedrally twinned. The twin components are related by a twofold axis around the vector 0.0034a* + 0.7058b* + 0.7084c*. Data integration of the twinned data was performed using CrysAlisPro, and a HKLF 5 file was made. The BASF scale factor refines to 0.2245(18).

$[Ni_2Cl_2(BnC_3S)_2]$ [**2**]: The structure is partly disordered. The two crystallographically independent dichloromethane solvent molecules in the asymmetric unit are found to be disordered over two orientations. The occupancy factors of the major components of the disorder refine to 0.864(2) and 0.881(3).

$[Ni_2(PyC_2S)_2]Br_2$ [**3**]Br_2: The asymmetric unit contains four crystallographically independent dinuclear cations and eight bromide anions. The structure is partly disordered. Two of the four dimers are disordered over two orientations, and the occupancy factors of the major components of the disorder refine to 0.643(8) and 0.722(5), respectively. Four of the eight Br^- counter ions are fully occupied (and ordered), whereas the remaining counter ions are found to be disordered over two, three or four positions. For those counterions, the sum of the occupancy factors was restrained to be equal to four using the SUMP instruction. The crystal lattice also contains some amount of unresolved electron density (most likely disordered and/or partially occupied lattice solvent molecules), whose contribution has been taken out in the final refinement.[46]

$[Ni_2(PyC_2S)_2]Br_2$ [**4**]Br_2: The structure is partly disordered. One of the two Br^- counter ions is disordered over two positions, and the occupancy factor of the major component of the disorder refines to 0.74(3). The crystal lattice also contains one very disordered MeOH lattice solvent molecule per asymmetric unit found at sites of twofold axial symmetry; its contribution has been taken out in the final refinement.[46] The crystal was not single but rather a composite of three crystals stuck together, and the two BASF scale factors refine to 0.146(2) and 0.1023(19).

2.4.4 Ligand precursors synthesis

N-Pyridylmethylbenzimidazole,[47] and the benzimidazolium ligand precursor salts $[HBnC_2Br]Br$ (**A)** and $[HBnC_3Br]Br$ (**B**)[25], $[HBnC_2SAc]Br$ (**C**) and $[HBnC_3SAc]Br$ (**D**),[26], $[HPyC_2Br]Br$ (**E**) and $[HPyC_2Br]Br$ (**F**)[27] were synthesized following literature methods.

$[HPyC_2SAc]Br$ (**G**):
A mixture of salt **E** (0.625 g, 1.6 mmol) and $KSCOCH_3$ (0.200 g, 1.8 mmol) in acetonitrile (10 mL) was stirred at room temperature for 16 h. The suspension was filtered, yielding a white powder. The white powder was washed with diethyl ether to get the pure product in a yield of 0.44 g (72%). ^{1}H NMR (300 MHz, DMSO-d_6) δ 10.02 (s, 1H, NCHN), 8.49 (d, J = 4.8 Hz, 1H, Ar-*H*), 8.17 (d, J = 8.4 Hz, 1H, Ar-*H*), 7.99 – 7.85 (m, 2H, Ar-*H*), 7.75 – 7.57 (m, 3H, Ar-*H*), 7.43 – 7.32 (m, 1H, Ar-*H*), 5.95 (s, 2H, N-CH_2-Py), 4.77 (t, J = 6.4 Hz, 2H,

NCH_2), 3.43 (t, J = 6.6 Hz, 2H, CH_2S), 2.28 (s, 3H, COCH_3). ^{13}C NMR (75 MHz, DMSO-d_6) δ = 149.63, 143.30, 137.57, 126.80, 126.71, 123.74, 122.74, 113.93, 113.84, 50.87, 46.19, 30.50, 27.83. The resonances of the four quaternary carbon atoms were not detected. ESI-MS found (calculated): $[M-Br]^+$ m/z 312.1 (312.1).

[HPyC$_3$SAc]Br (**H**):
A mixture of salt **F** (0.500 g, 1 mmol) and KSCOCH$_3$ (0.170 g, 1.2 mmol) in acetonitrile (10 mL) was stirred at room temperature for 48 h. The suspension was filtered, yielding a white powder, which was washed with a mixture of the filtrate and diethyl ether. The white powder was purified by column chromatography (Al_2O_3, dichloromethane, dichloromethane/methanol = 3:1) giving a yield of 0.37 g (75%). ^{1}H NMR (300 MHz, DMSO-d_6) δ 10.00 (s, 1H, NCHN), 8.48 (d, J = 5.6 Hz, 1H, Ar-H), 8.10 (d, J = 7.0 Hz, 1H, Ar-H), 8.00 – 7.84 (m, 2H, Ar-H), 7.74 – 7.60 (m, 3H, Ar-H), 7.38 (dd, J = 7.0, 5.3 Hz, 1H, Ar-H), 5.92 (s, 2H, N-CH_2-Py), 4.62 (t, J = 7.0 Hz, 2H, NCH_2), 2.93 (t, J = 7.3 Hz, 2H, CH_2S), 2.32 (s, 3H, COCH_3), 2.19 (p, J = 7.1 Hz, 2H, CH$_2$-CH_2-CH$_2$). ^{13}C NMR (75 MHz, DMSO-d_6) δ = 149.57, 137.54, 126.77, 126.63, 123.72, 122.75, 113.89, 113.79, 50.86, 45.77, 28.68, 25.23. The resonances of the four quaternary carbon atoms were too weak to be detected. ESI-MS found (calculated): $[M-Br]^+$ m/z 316.1 (316.1).

2.4.4 Synthesis of the nickel compounds

[Ni$_2$Cl$_2$(BnC$_2$S)$_2$] [**1**]:
Ligand precursor **C** (0.390 g, 1.0 mmol), anhydrous Ni(OAc)$_2$ (0.090 g, 0.5 mmol) and tetrabutylammonium bromide (2 g) were weighed into a 10 mL round-bottomed flask and dried for 3 hours at 60 ^{o}C under vacuum. Then the temperature of the flask was increased to 120 ^{o}C and kept constant for 24 hours. The mixture was allowed to cool to room temperature and then was triturated with H_2O (10 ml) and DCM (20 ml). The organic layer was separated, washed with brine and dried on sodium sulfate. Removal of the solvent resulted in a red solid in a yield of 85 mg (24%). Single crystals suitable for X-ray structure determination were obtained from a DCM solution of the complex. ^{1}H NMR (300 MHz, chloroform-d) δ 7.63 (d, J = 6.1 Hz, 4H, Ar-H), 7.47 – 7.01 (m, 14H, Ar-H), 6.68 (d, J = 15.5 Hz, 2H, N-CHH-Py), 5.69 (d, J = 15.6 Hz, 2H, N-CHH-Py), 5.07 (t, J = 13.0 Hz, 2H, CHHS), 4.78 (d, J = 13.4 Hz, 2H, NCHH), 2.89 (d, J = 12.4 Hz, 2H, NCHH), 1.36 (t, J = 11.8 Hz, 2H, CHHS). ^{13}C NMR (75 MHz, chloroform-d) δ 174.30, 136.45, 134.95, 133.94, 128.95, 128.10, 127.97, 123.28, 123.24, 111.39, 110.07, 52.32, 49.34, 24.19. Elemental analysis: $C_{32}H_{30}N_4S_2Ni_2Cl_2 \cdot CH_2Cl_2$: Calcd. C 49.06, H 3.99, N 6.93; Found 49.26, H 4.17, N 6.75. ESI-MS found (calculated): $[M-2Cl]^{2+}$ m/z 325.0 (325.03); $[M-Cl]^+$ m/z 685.3 (685.03).

[Ni$_2$Cl$_2$(BnC$_3$S)$_2$] [**2**]:
Ligand precursor **D** (0.405 g, 1.0 mmol), anhydrous Ni(OAc)$_2$ (0.177 g, 1.0 mmol) and tetrabutylammonium bromide (2 g) were weighed into a 10 mL round-bottomed flask and dried for 3 hours at 60 ^{o}C under vacuum. Then the temperature was increased to 120 ^{o}C and kept constant for 24 hours. The mixture was allowed to cool to room temperature and then

was triturated with H_2O (10 ml) and DCM (20 ml). The organic layer was separated, washed with brine and dried on sodium sulfate. Removal of the solvent resulted in a red solid, which was washed with diethyl ether, giving a yield of 50 mg (13%). Single crystals suitable for X-ray structure determination were obtained from a DCM solution. ^{1}H NMR (300 MHz, Dichloromethane-d_2) δ 7.85 (td, J = 13.6, 5.9 Hz, 2H, CH*H*S), 7.55 (d, J = 6.8 Hz, 4H, Ar-*H*), 7.49 – 7.29 (m, 8H, Ar-*H*), 7.25 – 7.07 (m, 6H, Ar-*H*), 6.56 (d, J = 15.6 Hz, 2H, N-CH*H*-Py), 5.53 (d, J = 15.6 Hz, 2H, N-C*H*H-Py), 5.12 (dd, J = 14.3, 6.6 Hz, 2H, NCH*H*), 2.93 (m, 2H, CH_2-CH*H*-CH_2), 2.12 (m, 4H, CH_2-C*H*H-CH_2, NC*H*H), 0.63 (td, J = 13.5, 4.9 Hz, 2H, C*H*HS). ^{13}C NMR (75 MHz, Dichloromethane-d_2) δ = 176.08, 136.67, 135.54, 133.79, 129.18, 128.39, 128.21, 123.40, 123.17, 111.40, 109.96, 51.94, 44.51, 23.84, 22.59. Elemental analysis: $C_{34}H_{34}N_4S_2Ni_2Cl_2 \cdot C_4H_{10}O$: Calcd. C 55.31, H 5.37, N 6.79; Found C 55.15, H 5.09, N 6.54. ESI-MS found (calculated): $[M-Cl]^+$ *m*/*z* 713.3 (713.06).

$[Ni_2(PyC_2S)_2]Br_2$ [**3**]Br_2:
Ligand precursor **G** (0.380 g, 0.8 mmol), anhydrous $Ni(OAc)_2$ (0.140 g, 0.8 mmol) and tetrabutylammonium bromide (1.5 g) were weighed into a 10 mL round bottom flask and dried for 3 hours at 80 °C under vacuum. Then the temperature was increased to 120 °C and kept for 48 hours. The mixture was allowed to cool to room temperature and then was triturated with H_2O (10 ml) resulting in a red solid. The solid was washed with a small amount of DCM and dried in vacuum, giving a yield of 75 mg of a red solid (18%). Crystals suitable for X-ray structure determination were obtained by slow evaporation of a degassed methanol solution under a flow of argon. ^{1}H NMR showed broad signals. ^{1}H NMR (300 MHz, DMSO-d_6) δ = 9.09, 8.13, 8.00, 7.91, 7.75, 7.57, 7.43, 6.16, 4.53, 2.13. Elemental analysis: $C_{30}H_{28}N_6S_2Ni_2Br_2 \cdot 1.5H_2O$: Calcd. C 42.85, H 3.72, N 9.99; Found C 42.55, H 3.40, N 9.99. ESI-MS found (calculated): $[M-2Br]^{2+}$ *m*/*z* 326.1 (326.03); [1/2M-Br+MeOH]$^+$ (mononuclear) *m*/*z* 358.1 (358.05).

$[Ni_2(PyC_3S)_2]Br_2$ [**4**]Br_2:
Ligand precursor **H** (0.405 g, 1.0 mmol), anhydrous $Ni(OAc)_2$ (0.180 g, 1.0 mmol) and tetrabutylammonium bromide (1.9 g) were weighed into a 10 mL round bottom flask and dried for 3 hours at 80 °C under vacuum. Then the temperature was increased to 130 °C and kept for 24 hours. The mixture was allowed to cool to room temperature and then was triturated with H_2O (10 ml) resulting in a red solid. The solid was washed with a small amount of DCM and dried in vacuum, giving a yield of 42 mg (10%). Crystals suitable for X-ray structure determination were obtained by slow evaporation of a degassed methanol solution under a flow of argon. ^{1}H NMR (300 MHz, DMSO-d_6) δ 8.88 (d, *J* = 5.3 Hz, 2H), 8.09 – 8.00 (m, 4H, Ar-*H*), 7.88 (d, *J* = 7.7 Hz, 2H, Ar-*H*), 7.76 (d, *J* = 8.0 Hz, 2H, Ar-*H*), 7.51 – 7.39 (m, 6H, Ar-*H*), 6.58 (d, *J* = 15.4 Hz, 2H, N-CH*H*-Py), 6.29 (d, *J* = 15.1 Hz, 2H, N-C*H*H-Py), 4.84 (broad, 2H), 4.67 (d, *J* = 12.8 Hz, 2H), 1.92 (broad, 4H), 1.43 (broad, 4H). ^{13}C NMR (75 MHz, DMSO-d_6) δ = 171.14, 154.93, 154.70, 140.08, 133.51, 133.33, 125.47, 125.29, 123.76, 111.31, 110.96, 50.25, 42.37, 27.18, 24.53. $C_{32}H_{32}N_6S_2Ni_2Br_2$

$3CH_3OH{\cdot}3H_2O$: Calcd. C 42.37, H 5.08, N 8.47; Found C 42.76, H 5.13, N 8.41. ESI-MS found (calculated): $[M-2Br]^{2+}$ *m*/*z* 340.0 (340.04); $[M-Br]^{+}$ *m*/*z* 759.0 (759.00).

2.5 Acknowledgement

S. Luo gratefully acknowledges a grant from the Chinese Scholarship Council (no. 201306410011). We thank Mr. J.M.M van Brussel for ESI-MS measurements.

2.6 References

[1] B. Rausch, M.D. Symes, G. Chisholm, L. Cronin, *Science* 2014, 345, 1326-1330.
[2] D.L. DuBois, *Inorg. Chem.* 2014, 53, 3935-3960.
[3] T.R. Simmons, G. Berggren, M. Bacchi, M. Fontecave, V. Artero, *Coord. Chem. Rev.* 2014, 270, 127-150.
[4] P. Tong, W. Xie, D. Yang, B. Wang, X. Ji, J. Li, J. Qu, *Dalton Trans.* 2016, 45, 18559-18565.
[5] S. Canaguier, V. Fourmond, C.U. Perotto, J. Fize, J. Pecaut, M. Fontecave, M.J. Field, V. Artero, *Chem. Commun.* 2013, 49, 5004-5006.
[6] L. Gan, T.L. Groy, P. Tarakeshwar, S.K.S. Mazinani, J. Shearer, V. Mujica, A.K. Jones, *J. Am. Chem. Soc.* 2015, 137, 1109-1115.
[7] D. Brazzolotto, M. Gennari, N. Queyriaux, T.R. Simmons, J. Pecaut, S. Demeshko, F. Meyer, M. Orio, V. Artero, C. Duboc, *Nat Chem* 2016, 8, 1054-1060.
[8] I.K. Pandey, S.M. Mobin, N. Deibel, B. Sarkar, S. Kaur-Ghumaan, *Eur. J. Inorg. Chem.* 2015, 2875-2882.
[9] A. Mondragón, M. Flores-Alamo, P.R. Martínez-Alanis, G. Aullón, V.M. Ugalde-Saldívar, I. Castillo, *Inorg. Chem.* 2015, 54, 619-627.
[10] K. Hou, H.T. Poh, W.Y. Fan, *Chem. Commun.* 2014, 50, 6630-6632.
[11] L.-C. Song, H. Tan, F.-X. Luo, Y.-X. Wang, Z. Ma, Z. Niu, *Organometallics* 2014, 33, 5246-5253.
[12] E.I. Musina, V.V. Khrizanforova, I.D. Strelnik, M.I. Valitov, Y.S. Spiridonova, D.B. Krivolapov, I.A. Litvinov, M.K. Kadirov, P. Lonnecke, E. Hey-Hawkins, Y.H. Budnikova, A.A. Karasik, O.G. Sinyashin, *Chem. -Eur. J.* 2014, 20, 3169-3182.
[13] R.M. Stolley, J.M. Darmon, M.L. Helm, *Chem. Commun.* 2014, 50, 3681-3684.
[14] M.L. Helm, M.P. Stewart, R.M. Bullock, M.R. DuBois, D.L. DuBois, *Science* 2011, 333, 863-866.
[15] D. Morvan, J.-F. Capon, F. Gloaguen, A. Le Goff, M. Marchivie, F. Michaud, P. Schollhammer, J. Talarmin, J.-J. Yaouanc, R. Pichon, N. Kervarec, *Organometallics* 2007, 26, 2042-2052.
[16] C.C. McCrory, C. Uyeda, J.C. Peters, *J. Am. Chem. Soc.* 2012, 134, 3164-3170.
[17] P.A. Jacques, V. Artero, J. Pecaut, M. Fontecave, *Proc. Natl. Acad. Sci. U. S. A.* 2009, 106, 20627-20632.
[18] N. Kaeffer, A. Morozan, V. Artero, *J. Phys. Chem. B* 2015, 119, 13707-13713.
[19] S.M. Laga, J.D. Blakemore, L.M. Henling, B.S. Brunschwig, H.B. Gray, *Inorg. Chem.* 2014, 53, 12668-12670.
[20] P.D. Tran, J. Barber, *Phys. Chem. Chem. Phys.* 2012, 14, 13772-13784.
[21] K. Kawano, K. Yamauchi, K. Sakai, *Chem. Commun.* 2014, 50, 9872-9875.
[22] M. van der Meer, E. Glais, I. Siewert, B. Sarkar, *Angew. Chem. Int. Ed.* 2015, 54, 13792-13795.

[23] S. Luo, M.A. Siegler, E. Bouwman, *Eur. J. Inorg. Chem.* 2016, 4693-4700.
[24] S. Jiang, T. Zhang, X. Zhang, G. Zhang, L. Hai, B. Li, *RSC Advances* 2016, 6, 84139-84148.
[25] D. Yuan, H.V. Huynh, *Organometallics* 2010, 29, 6020-6027.
[26] D. Yuan, Q. Teng, H.V. Huynh, *Organometallics* 2014, 33, 1794-1800.
[27] A.K. Lal, M.D. Milton, *Tetrahedron Lett.* 2014, 55, 1810-1814.
[28] M.H. Reineke, M.D. Sampson, A.L. Rheingold, C.P. Kubiak, *Inorg. Chem.* 2015, 54, 3211-3217.
[29] D. Yuan, H.V. Huynh, *Inorg. Chem.* 2013, 52, 6627-6634.
[30] R. Jothibasu, K.-W. Huang, H.V. Huynh, *Organometallics* 2010, 29, 3746-3752.
[31] T. Kosterke, T. Pape, F.E. Hahn, *Chem. Commun.* 2011, 47, 10773-10775.
[32] H. Vinh Huynh, R. Jothibasu, *Eur. J. Inorg. Chem.* 2009, 1926-1931.
[33] H.V. Huynh, C. Holtgrewe, T. Pape, L.L. Koh, E. Hahn, *Organometallics* 2006, 25, 245-249.
[34] J.C. Bernhammer, H.V. Huynh, *Organometallics* 2014, 33, 5845-5851.
[35] E.M. Matson, G. Espinosa Martinez, A.D. Ibrahim, B.J. Jackson, J.A. Bertke, A.R. Fout, *Organometallics* 2015, 34, 399-407.
[36] D.H. Brown, B.W. Skelton, *Dalton Trans.* 2011, 40, 8849-8858.
[37] G.E. Martinez, C. Ocampo, Y.J. Park, A.R. Fout, *J. Am. Chem. Soc.* 2016, 138, 4290-4293.
[38] P. Zhang, M. Wang, Y. Yang, T. Yao, L. Sun, *Angew. Chem. Int. Ed.* 2014, 53, 13803-13807.
[39] M.P. Stewart, M.-H. Ho, S. Wiese, M.L. Lindstrom, C.E. Thogerson, S. Raugei, R.M. Bullock, M.L. Helm, *J. Am. Chem. Soc.* 2013, 135, 6033-6046.
[40] R. Tatematsu, T. Inomata, T. Ozawa, H. Masuda, *Angew. Chem. Int. Ed.* 2016, 55, 5247-5250.
[41] C. Costentin, J.-M. Saveant, *Chemelectrochem* 2014, 1, 1226-1236.
[42] J.M. Saveant, *Chemelectrochem* 2016, 3, 1967-1977.
[43] E.S. Wiedner, R.M. Bullock, *J. Am. Chem. Soc.* 2016, 138, 8309-8318.
[44] C. Costentin, S. Drouet, M. Robert, J.-M. Savéant, *J. Am. Chem. Soc.* 2012, 134, 11235-11242.
[45] G.M. Sheldrick, *Acta Cryst. A* 2008, 64, 112-122.
[46] A.L. Spek, *Acta Cryst. D* 2009, 65, 148-155.
[47] J. Dinda, S.D. Adhikary, S.K. Seth, A. Mahapatra, *New J. Chem.* 2013, 37, 431-438.